Carbon 233 (2025) 119873

Contents lists available at ScienceDirect

Carbon

journal homepage: www.elsevier.com/locate/carbon

RGB photoluminescence from single-component hydrocarbon single-crystals: Revealing excited-state dynamics in organic semiconductors

Takeshi Nakagawa [a,*], Shaohua Fu [b], Kejun Bu [a], Dong Wang [a], Martina Vrankić [c], Philip Dalladay-Simpson [a], Xia Yin [a], Jianbo Zhang [a], Yonggang Wang [a], Xujie Lü [a], Jimin Zhao [b,**], Ho-kwang Mao [a], Yang Ding [a,***]

[a] Center for High Pressure Science and Technology Advanced Research, 10 Xibeiwang East Road, Haidian District, Beijing, 100094, PR China
[b] Beijing National Laboratory for Condensed Matter Physics, Institute of Physics, Chinese Academy of Sciences, Beijing, 100190, PR China
[c] Division of Materials Physics, Ruđer Bošković Institute, Bijenička 54, 10000, Zagreb, Croatia

ARTICLE INFO

Keywords:
Polycyclic aromatic hydrocarbons
Single-crystal
RGB luminescence
Excited-state dynamics
Excited-state absorption

ABSTRACT

The development of single-component organic materials that exhibit tunable red, green and blue (RGB) luminescence under ambient conditions can pave the way of materials with tailored photophysical properties. The optical behavior of such organic materials is largely determined by their excited-state dynamics of the excitons, which are formed when electrons are excited in the material. The excited-state dynamics of an organic molecules can be sensitively tuned, where even marginal variations in crystal morphology and molecular arrangement can drastically modify their optical behavior. Herein, we report a discovery of π-conjugated single-component system that can exhibit the RGB emission. This was realized by altering the morphological crystal dimensionality of a highly tunable single-component hydrocarbon coronene molecule in a single-step crystallization processes into 1D wire, 2D plate, and 3D rod, without introducing additional components or varying external stimuli. Time-resolved photoluminescence (PL) and transient absorption spectroscopy revealed the excited-state absorption (ESA) and self-trapped exciton (STE) formation in the excited electrons in 1D wire crystal plays a key role in emission color change from blue to green. Furthermore, static PL and absorption spectroscopy and single-crystal XRD revealed the dimerization of coronene results in significant reduction of optical band-gap energy and red shift into red emission band. We elucidated the complex relationship between excited-state dynamics and crystal structure of the coronene crystals. Our work presents a novel strategy for tuning the optical properties of single-component organic materials through crystal engineering, offering new possibilities for the development of advanced organic semiconducting devices.

1. Introduction

Solid-state organic luminescent materials with tunable optical properties have found increased research importance for their potential applications to organic optoelectronic devices, such as organic light-emitting diodes (OLEDs), organic lasers, and organic photovoltaics [1–6] A key component of such electronic devices is semiconductors based on organic molecules, where their properties are largely determined by formation of excitons and their dynamics in the material [7–10] Key challenges in this field are found in the design and synthesis of efficient and color-tunable organic materials and also in elucidation of their complex excited-state dynamics that are critical for boosting the functionality of optoelectronic devices. Significant amount of research efforts has been placed over the years to develop color-tunable materials with a wide emission range and on the investigations of their mechanisms [11–15] In particular, single-component organic system that can exhibit red, green, and blue (RGB) luminescence under ambient conditions without the need for additional components or varying external stimuli, which will allow systematic investigations on crystal structures and photophysical processes. However, achieving RGB emission in a single-component organic material is challenging due to the significant differences in emission wavelengths that vary over a wide range of

* Corresponding author.
** Corresponding author.
*** Corresponding author.
E-mail address: takeshi.nakagawa@hpstar.ac.cn (T. Nakagawa).

https://doi.org/10.1016/j.carbon.2024.119873
Received 15 August 2024; Received in revised form 27 November 2024; Accepted 27 November 2024
Available online 28 November 2024

energy bands.

Organic molecular crystals offer a unique platform for exploring the relationship between crystal structure, molecular arrangements, polymorphism, morphology, and optical properties. The photophysical properties of single-component materials are highly sensitive to subtle changes in molecular packing and intermolecular interactions, enabling the tuning of optical behavior through crystal engineering [16] Recent studies have demonstrated the potential of controlling the emission properties of organic crystals by manipulating their morphology and dimensionality [17,18] In the excited-state of organic molecule, singlet excitons are generated with each absorbed photon, which undergo various relaxation processes involving either non-radiative or radiative paths. Different photophysical processes have distinct excited-state dynamics [19–21] and their electron transition features can be probed via absorption or photoluminescence (PL) spectroscopy. The excited-state dynamics of an organic materials can be sensitively tuned, where even marginal modifications of crystal morphologies can drastically alter their optical behaviour. The challenge here is to find appropriate crystal engineering protocols to fabricate high-quality crystals that have the desired properties.

In this study, we report the discovery of RGB emission from three single-crystals that are composed only of coronene, well known member of polycyclic aromatic hydrocarbon (PAH) molecule with high degree of π-conjugated structure. Two optically yellow crystals were grown in two different crystal morphology, namely, short and thick three-dimensional (3D) rod-crystal (typical dimension of the crystal: 1.0 mm × 0.3 mm × 0.13 mm), and long and thin one-dimensional (1D) wire-crystal (13.0 mm × 0.05 mm × 0.02 mm). Single-crystal XRD revealed that they possess identical 3D γ-herringbone crystal structure but exhibit different emission band under UV-light irradiation, blue and green, respectively. The third crystal is optically red, short and flat two-dimensional (2D) plate-crystal (2.4 mm × 0.13 mm × 0.05 mm), formed by coronene dimerization, which exhibit red emission band (Scheme 1). Through a combination of time-resolved and static photoluminescence (PL) and absorption spectroscopy, we elucidated the roles of morphological dimensionality and dimerization on the excited-state dynamics and optical band-gap energies. Our findings provide new insights into the intricate relationship between morphological dimensionality, molecular interaction, excited-state dynamics and photophysical properties in hydrocarbon single-crystals. This work presents a novel strategy for tuning the optical properties of single-component organic materials through crystal engineering, paving a way for the rational design of efficient, color-tunable organic optical devices.

2. Experimental details

2.1. Crystal preparation

Starting material of coronene ($C_{24}H_{12}$) was purchased from TCI Chemicals (>98 %) and purified by sublimation. Single-crystals of 3D rod and 1D wire coronene were obtained by crystallization technique. As received coronene was dissolved in anhydrous tetrahydrofuran (THF) and heated at 350 K with stirring on a magnetic plate. Anhydrous hexane was slowly added on top of the THF solution to form a layer to induce the crystallization of 3D rod by diffusion process. The 1D wire single-crystals were obtained by dissolving coronene in anhydrous toluene

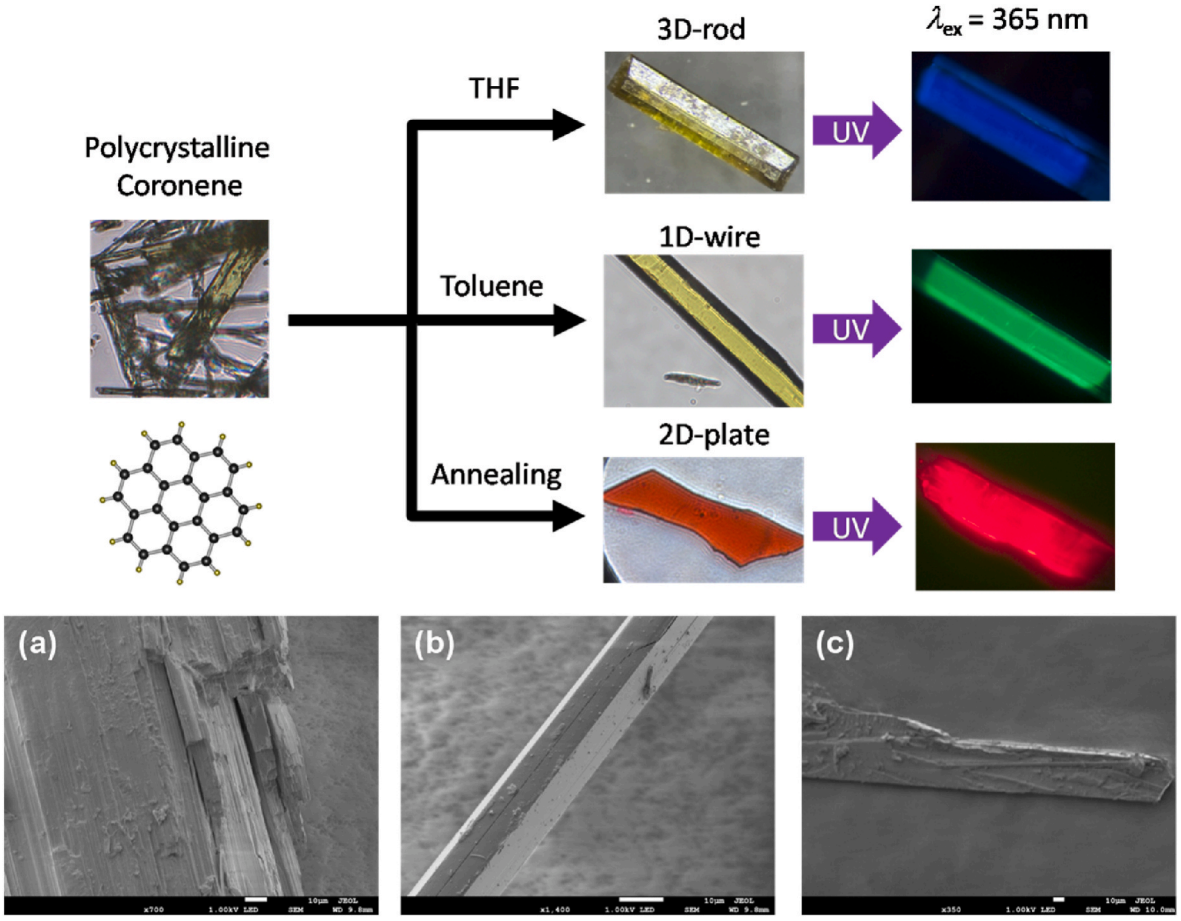

Scheme 1. Optical images, PL micrograph and SEM images of coronene single-crystals of (a) 3D rod with blue emission and (b) 1D wire with green emission and (c) 2D plate coronene dimer single-crystals with red emission, obtained by single excitation laser (λ_{ex} = 365 nm). SEM images focused on the broken surface of the crystal showing a layered 3D structure (a) and no layering 1D and 2D structure (b and c). Black solid arrows indicate process employed for single-crystal preparation.

and heating to 370 K with stirring on the magnetic plate and cooling down to room temperature (1 K/min). Single-crystal coronene dimer 2D plates were obtained by the vapor phase fusion reaction of coronene molecules. The sublimed coronene powder was placed in a long Pyrex tube and annealed for 5 h in a tube furnace (773 K) with a temperature gradient (−20 K) to separate dicoronylene from pristine coronene. The furnace was cooled slowly (2 K/h) to room temperature to obtain red needle-like crystals.

2.2. Single-crystal XRD measurements

Single-crystal diffraction data for both coronene and dicoronylene were collected using a Bruker D8 VENTURE PHOTON II X-ray diffractometer with Photon 100 CMOS detector equipped with a Microfocus Incoatec Ims 3.0, Mo-target X-ray tube ($\lambda = 0.71073$ Å), and a multilayer optical monochromator at room temperature. Data reduction and integration were performed with the Bruker software package SAINT. The structure was solved by SHELXT (version 2014/5) and refined using the Bruker SHELXL program (version 2016/6) by full matrix least squares procedures. The integration of the data using a monoclinic unit cell resulted in a maximum θ angle of 24.8° (0.85 Å resolution).

2.3. Raman spectroscopy

Raman measurements were performed using the MonoVista CRS + system (Spectroscopy & Imaging) with a laser excitation of 532, 633 and 785 nm (1.03 mW laser power). A grating with 1200 grooves/mm was used throughout the experiment. The laser beam was focused on the sample with a 20 × objective lens, resulting in 10 μm a laser spot. Raman spectroscopy with 1064 nm laser excitation was performed using a Bruker IFS 66 instrument with a FRA 106 Raman module attachment and a Nd^{3+}/YAG laser. Laser power, exposure time, and number of accumulations were adjusted for each excitation laser used, and spectra were recorded over the wave number range of 15–3600 cm^{-1}.

2.4. Scanning electron microscopy

The morphology of the materials was investigated using a field emission scanning electron microscope (FESEM, JEOL JSM-7900F). Thermal (Schottky) field emission gun with an accelerating voltage of 10.0 kV was used and images were recorded with an Energy-dispersive X-ray spectroscopy (EDS) detector (Oxford Instruments Aztec X-max50).

2.5. UV–vis absorption and photoluminescence spectroscopy

Measurements of UV–Vis absorption, photoluminescence spectra, optical image, and fluorescence images were conducted using a home-designed spectroscopy (Gora-UVN-FL, Ideaoptics, Shanghai), with an integrated micro-region spectroscopy system. The UV–Vis absorption spectra were recorded using a xenon light source (SLS201L, Thorlabs, USA) in the range between 300 nm and 1100 nm with the laser beam was focused on the surface of the sample with 20 × objective lens (0.42 NA, Mitutoyo, Japan), resulting in a laser spot of about 40 μm diameter. Laser power adjustment was achieved through a neutral-density filter. Single-crystals (typical dimensions length:width:thickness of 60 × 50 × 10 μm^3) were placed on 400 μm culet-sized low-fluorescent flat diamond surface. Background signals were obtained first on the diamond surface and subtracted. Absorption measurements were recorded for transmitted light. The band gap of coronene is determined by extrapolating the linear intercept of the $\alpha^{1/2}$ *vs* hν curve, where α is the absorption coefficient, h is Planck's constant, and ν is the frequency of the photon. Fluorescence images were collected under irradiation with UV light with an accumulation time of 200 μs. The time-resolved PL spectra were acquired utilizing a custom-built transient state spectroscopy system (Timetechspectra, China) A 405 nm ps laser, selected from a supercontinuum laser source (SC-OEM, Yangtze Soton Laser, China) via a bandpass filter, operated at a repetition rate of 10 MHz with a pulse width of approximately 100 ps. The time-resolved PL lifetime decay kinetics were captured and analyzed employing a time-correlated single photon counting module in conjunction with a single photon avalanche diode (SPAD) detector (id100-20, IDQ, Switzerland), featuring an instrument response function of around 180 ps. The decay curves were fitted using the double exponential function

$$I(t) = A_1\, exp\left(-\frac{t}{\tau_1}\right) + A_2\, exp\left(-\frac{t}{\tau_2}\right)$$

where I is the luminescence intensity, τ_1 and τ_2 are the components of the decay time, and A_1 and A_2 are the corresponding fitting parameters.

2.6. PL quantum yield

The PL quantum yield and excitation spectra were measured using the FS5 spectrofluorometer (Edinburgh Instruments Ltd.) equipped with a SC-30 Integrating Sphere Module. Al_2O_3 was used as the absorption reference.

2.7. Femtosecond transient absorption spectroscopy

Femtosecond transient absorption spectra with temporal resolution of 150 fs were carried out by a commercial femtosecond TAS system. (HELIOS, Ultrafast Systems). To generate the pump pulse, the fundamental 800 nm pulse from a regenerative amplifier (1 KHz, 80 fs, 2.5 mJ per pulse, Coherent, Astrella), seeded by an oscillator (80 MHz, 35 fs, Coherent Vitara-S), was applied to pump an optical parametric amplifier (Coherent, OperA Solo). The continuum of white light, which was generated by focusing a small fraction of the 800 nm output of the Astrella onto a sapphire crystal in HELIOS, served as the probe light.

We used 400 nm light as a pump to excite the coronene crystal. The excitation densities and pump fluence were kept identical in all TA experiment to compare the carrier dynamics. Here, the TA signals are divided into ground-state bleaching (GSB) signals that stem from photoinduced bleaching due to a state filling effect and excited-state absorption (ESA) signals, which refer to photoinduced absorption of excited states. Single-crystals were placed on quartz substrates. To spatially resolve the three different crystals, the 400 nm pump and white probe light are focused onto the sample with 20 × objective lens, and the beam size of pump and probe laser are focused down to 5 μm and 20 μm, respectively. The change of absorbance at different delay time is recorded by Helios system software to capture the dynamic information of the excited state of the single-crystals.

3. Results and Discussion

Three single-crystals were prepared from commercially available coronene via two distinct methods: recrystallization in solvents and thermal annealing. The optically yellow 3D rod crystals were obtained by dissolving coronene in anhydrous tetrahydrofuran (THF) and then recrystallized through diffusion process. The other yellow 1D wire crystals were formed through dissolving coronene in anhydrous toluene and recrystallization. Single-crystal X-ray diffraction (ScXRD) reveals that both crystals exhibit a monoclinic γ-herringbone assembly with space group $P2_1/n$ and their lattice parameters are in good agreement with previously published results for γ-polymorph coronene [22] The optically red 2D plate crystals were obtained by the vapor phase fusion reaction of the as received coronene powder annealed at 800 K in vacuum. The ScXRD showed that these crystals adopt a different β-herringbone arrangement with space group $P2_1/c$, confirming previous findings of dimerized coronene ($C_{48}H_{20}$) [23] The crystal structures, lattice parameters, and nearest neighbor (nn) distances and angles are summarized in Table 1 and their molecular packing structure can be found in Fig. S1, detailed refined XRD data can be found in Tables S2–S4.

Table 1
Summary of $C_{24}H_{12}$ and $C_{48}H_{20}$ unit cell metrics and reliability factors obtained from refinements of ScXRD laboratory data (λ = 0.71073 Å) at ambient conditions.

Crystal morphology	3D rod	1D wire	2D plate
Chemical formula	$C_{24}H_{12}$	$C_{24}H_{12}$	$C_{48}H_{20}$
polymorph	γ-herringbone	γ-herringbone	β-herringbone
M_r	300.25	300.25	596.51
Crystal system	monoclinic	monoclinic	monoclinic
Space group	$P2_1/n$	$P2_1/n$	$P2_1/c$
a (Å)	10.0879(5)	10.113(5)	10.3940(8)
b (Å)	4.6976(2)	4.704(2)	3.8402(3)
c (Å)	15.6585(8)	15.722(7)	31.990(3)
β (°)	106.005(2)	106.06(2)	90.248(2)
V (Å^3)	713.28(6)	718.7(5)	1276.89(17)
Z	2	2	2
ρ_{calcd} (g/cm^3)	1.399	1.399	1.552
***R* indices**	R_1 = 3.45 %, $_wR_2$ = 9.31 %	R_1 = 3.15 %, $_wR_2$ = 2.18 %	R_1 = 2.4 %, $_wR_2$ = 7.4 %
***nn C–C distance* (Å)**	3.491(6)	3.490(7)	3.474(3)
***nn H–H distance*(Å)**	2.5745(4)	2.5851(5)	2.5281(2)
***Herringbone angle*(°)**	96.33(11)	96.69(10)	48.6(3)

As shown in Scheme 1, SEM and optical micrographs revealed the unique morphological features of these crystals. In particular, Scheme 1 (a) shows the layered structure of the 3D rod with conceivably hundreds of nm-thick layers of coronene, whereas Scheme 1(b) displays a non-layered thin structure with smooth crystal edges. Scheme 1(c) shows that 2D plate crystals possess thin and flat morphology, but do not have a layered edges.

We obtained Raman spectra of three crystals using lasers with excitation wavelengths of 1064, 633, and 532 nm. The profiles for the 3D rod and 1D wire are identical and aligned with existing literature [24] The 3D rod crystals yielded the best spectra using a 633 nm laser source, while the 1D wire crystals required a 1064 nm laser source to avoid strong fluorescence interference, which clearly indicates the optical properties of the coronene crystal can be largely tuned by crystal morphology. The Raman spectra for the 2D plate crystal can also only be acquired using 1064 nm laser source by avoiding strong fluorescence, and the obtained spectrum was also found to be in good agreement with previous report on dicoronylene [25] Full Raman spectrums for all three single-crystals are available in supplementary information, Fig. S2.

Fig. 1a–c displays the static ultraviolet–visible (UV–vis) absorption and PL spectra of three crystals measured under ambient conditions. The UV–vis absorption spectrum reveals a single, sharp absorption edge for both the 3D rod and 2D plate, attributed to the transition from the highest occupied molecular orbital (HOMO) to the lowest unoccupied molecular orbital (LUMO). The absorption maxima are located at 412 nm and 540 nm for the 3D rod and 2D plate, respectively. Using the Kubelka-Munk plots [26], the optical band gap between the singlet ground state S(0) and the first excited state S(1) is estimated to be 2.82 eV for the 3D rod and 2.20 eV for the 2D plate. Conversely, the 1D wire presents three distinct absorption edges, with maxima at 404 nm, 430 nm, and 464 nm, indicating that an incoming photon induces the population of the higher excited states from the singlet ground state. The optical band gaps estimated from the observed absorption edges are 2.62, 2.82, and 2.94 eV.

As seen by the PL micrograph under UV light, 3D rod coronene exhibits a blue emission, and the PL spectrum shows emission bands in the visible range between 415 and 650 nm (Fig. 2). Maximum emission intensity is observed at λ_{em} = 459 nm (E_{em} = 2.70 eV) as a result of the electronic transition from the lowest excited energy state to the ground state. The emission lifetime was determined from PL lifetime measurements by fitting transient fluorescence decay to a double exponential function (Fig. 3(left)). The decay spectrum for the 3D rod is divided into prompt (τ_p = 9.55(4) ns, relative amplitudes = 89.7(2)%) and delayed (τ_d = 39.6(3) ns, relative amplitudes = 10.4(2)%). The PL micrograph for 1D wire crystals exhibits a green emission and the PL spectrum shows emission band spanning 450–700 nm. The emission lifetimes of the 1D wire are τ = 10.0(2) ns and 46.2(2) ns, with relative amplitudes of 28.0(2)% and 72.0(2)%, respectively. It should be noted that, the typical fluorescence lifetime that only involves single-excitons are less than 10 ns, but phosphorescence and thermally activated delayed fluorescence lifetimes that involves triplet-excitons are typically longer than 1 μs. [27] Based on our experimental observations, we suggest that the nature of the PL emission of 1D wire is formed by two distinctive bands, where the fast component can be assigned to a prompt resonance-free exciton (FE) luminescence band, while the slow component can be assigned to a Stokes-shifted delayed fluorescence (DF) involving self-trapped exciton (STE) luminescence band. The PL quantum yield (PLQY) for this crystal was estimated as 15.3 %. The PL micrograph of a 2D plate crystal exhibits a red emission, the PL spectrum shows broad emission bands in the 570–870 nm range and the emission lifetime was determined to be τ = 8.39(3) ns. This significantly large red-shift and band-gap closure are attributed to the changes in crystal structure due to dimerization of coronene molecule [28] Fig. 3 (left panels) presents the transient PL collected under uniform conditions for all three crystals, and their fitted parameters are summarized in Table S1. The PL spectrum for three crystals correlate well with the observed RGB emission, more specifically, they can be converted into Comission Internationale de l'Eclairage (CIE) coordinates (x, y); (0.22, 0.21), (0.25, 0.48), and (0.56, 0.31), respectively, as illustrated in Fig. 2 (right panel).

In our exploration of the excited-state dynamics across the single-crystals, we employed femtosecond transient absorption spectroscopy. A pump wavelength of 400 nm was used to excite the crystal and a probe wavelength in the range of 450–780 nm was utilized to detect the change of absorbance, maintaining identical pump fluence of ~130 μJ/cm^2 across all experiments. Broadband excited state absorption (ESA) features of all three crystals, which shows an exponential intensity decay in the observation window, are depicted in Fig. 3. Notably, the 1D wire ESA signal (Fig. 3b) exhibits a marked red-shift relative to the 3D rod (full spectrum in Fig. S5). This shift corresponds with the Stokes shifted peak evident in PL emission, suggesting 1D wire coronene's access to the STE band. However, the observed ESA signals lack the specificity for distinct energy level assignments. In order to study the relaxation dynamics of the excited state, the decay curves and corresponding single- and three-exponential function fitting results are plotted (Fig. 3-right panels). The 1D wire's ESA signal lifetime (τ~8494 ps) stands out as being approximately 4000 times longer than that of the 2D-plate (τ~2.3 ps) and 6.5 times longer than that of 3D rod (τ~1295 ps). The measured time constant in the TA spectroscopy reflects the lifetime of the relevant excited states in the three different crystals and shed light on the possible recombination mechanism in the different crystals under the same excitation condition. Extended lifetime indicates that each exciton's residence time in that state is significantly long and that will lead to the enhancement of singlet-exciton population in the higher excited-state of the 1D wire. The excitons in the higher excited-state must relax, usually via non-radiative decay, to the meta-stable state, which in this case, STE state. Stimulated emission resulting from the fact that more excitons are available in the STE state than in the lower state where absorption of photons would most likely occur. Conversely, the 2D plate's ESA signal shows a significant red-shift attributed to coronene dimerization with very short lifetime, which indicates that exciton-exciton annihilation may occur due to coronene dimerization.

The nature of the luminescence can be first classified into one of two photophysical processes, fluorescence and phosphorescence, which have been well established during the past 60 years. Singlet excitons are generated with each absorbed photon in the excited states of organic

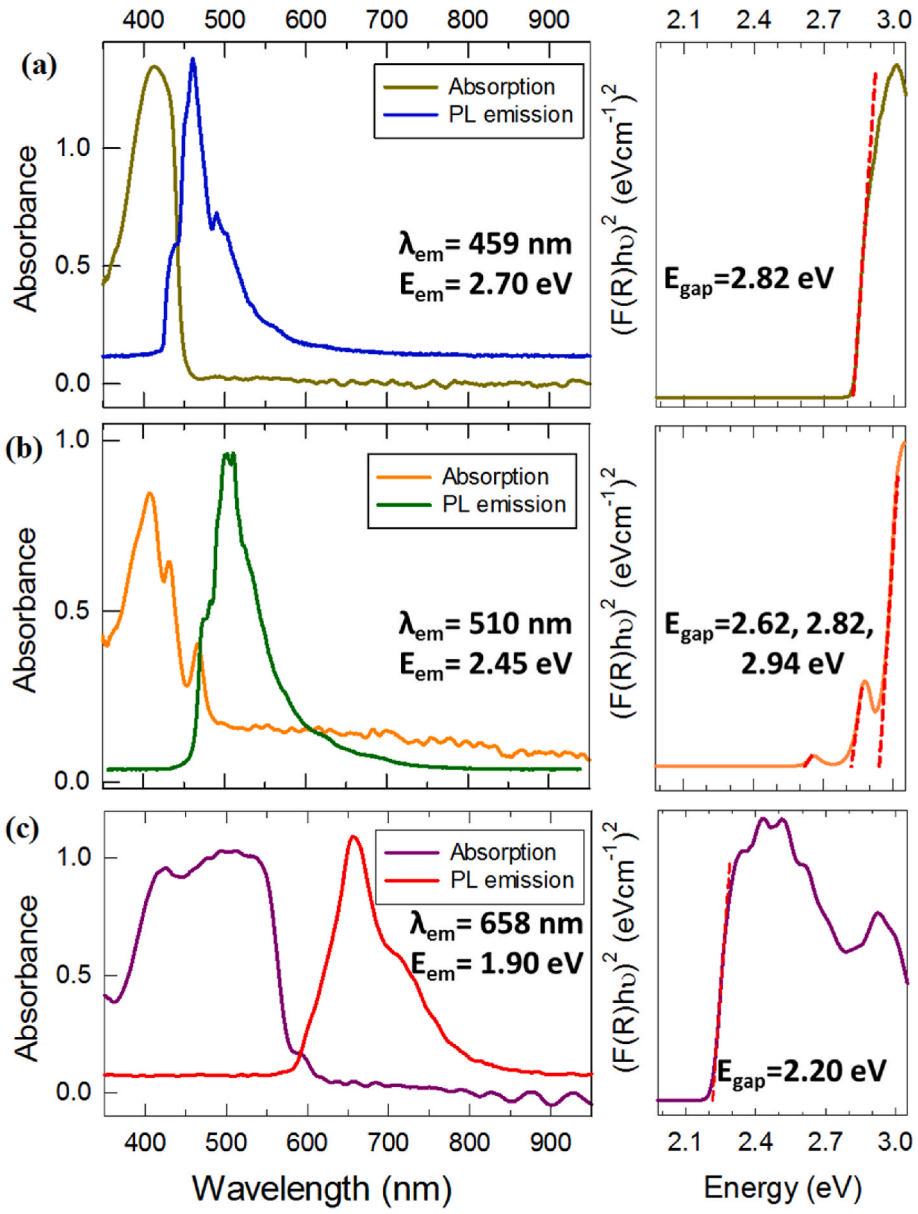

Fig. 1. Static UV–vis absorption and PL spectra of three single-crystals of (a) 3D rod (b) 1D wire and (c) 2D plate obtained under ambient conditions. PL emission spectra were obtained by single excitation wavelength, 405 nm. (A colour version of this figure can be viewed online.)

molecules, followed by the generation of triplet excitons via a non-radiative intersystem crossing (ISC). The fluorescence emission is observed during rapid decay of the singlet excitons, while phosphorescence results from the direct radiative decay of triplet excitons. The fluorescence is most commonly produced in organic aromatic compounds, as pure organic molecules do not have a mechanism to directly harvest triplet excitons, which generally relax to the ground state via non-radiative decay [29] Indeed, the RGB emissions observed in this study are all predominantly categorized under fluorescence. While the decay time of blue and red emission are less than 10 ns with the emission energy slightly lower than the band-gap energy, the green emission from 1D wire exhibits slightly longer decay time of 46 ns with the emission band-gap energy of 2.45 eV, which is much smaller than the band-gap. In fact, the emission band-gap energy is located exactly halfway between emission band-gap energy of singlet excited state (2.70 eV) and triplet excited state (2.20 eV) of coronene [30] It is therefore clear that this green emission is not a direct decay process from single/triplet excited state, but rather a DF via meta-stable STE state. It has been thought that the photophysical properties of an organic crystal is determined only by the intermolecular interactions, so that the same molecules in the same arrangement should produce identical optical properties. Surprisingly, both 3D and 1D coronene crystal structures are identical (Figs. S6 and S7), yet the absorption and emission bands differ significantly.

A previous study reported the observation of different fluorescence profiles in a naturally-occurring organic crystal, karpatite, and laboratory-grown crystalline coronene that are identical in composition. In their study, the blue fluorescence observed in karpatite is due to STE formed in their excited-state due to nano-texture in the structure of the crystals, while the loss of nano-texture leads to larger potential barrier preventing the access to the STE state in the laboratory-grown coronene crystals, resulting in green emission [31] Another study reported the simultaneous observation of FE and STE luminescence in coronene crystallized in thin needles, with STE assigned to the green emission band at 550 nm [32] Therein, coronene is classified as a 3D system with strong exciton-phonon coupling, in which FE from STE are separated by a self-trapping barrier. Theoretical calculations of the relaxed state energy of one- two- and three-dimensional organic crystals indicate that in a 3D system with strong electron-phonon coupling, a double well

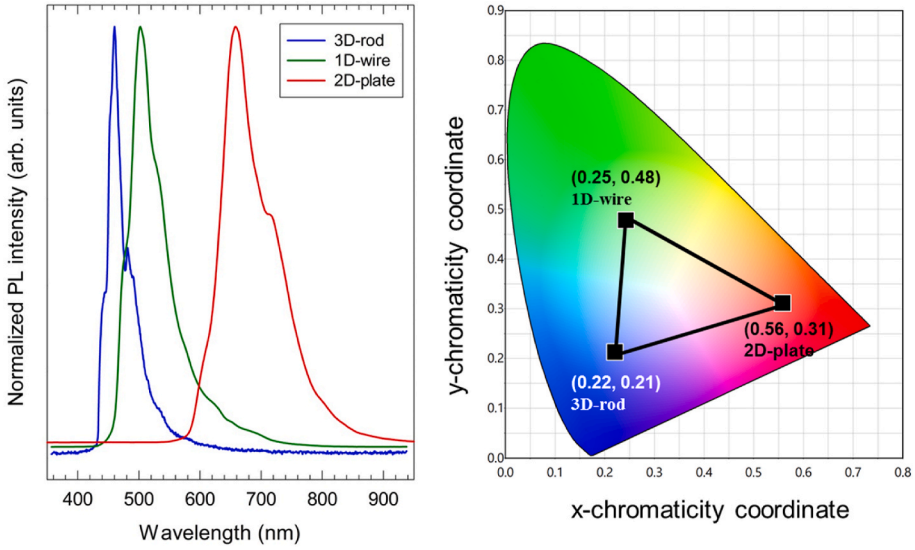

Fig. 2. Normalized PL spectra of 3D rod (blue), 1D wire (green) and 2D plate (red) single-crystals using UV irradiation (excitation laser wavelength $\lambda = 365$ nm) under ambient conditions in air. (right) Calculated CIE coordinates from the PL spectra of the three crystals. (For interpretation of the references to color in this figure legend, the reader is referred to the Web version of this article.)

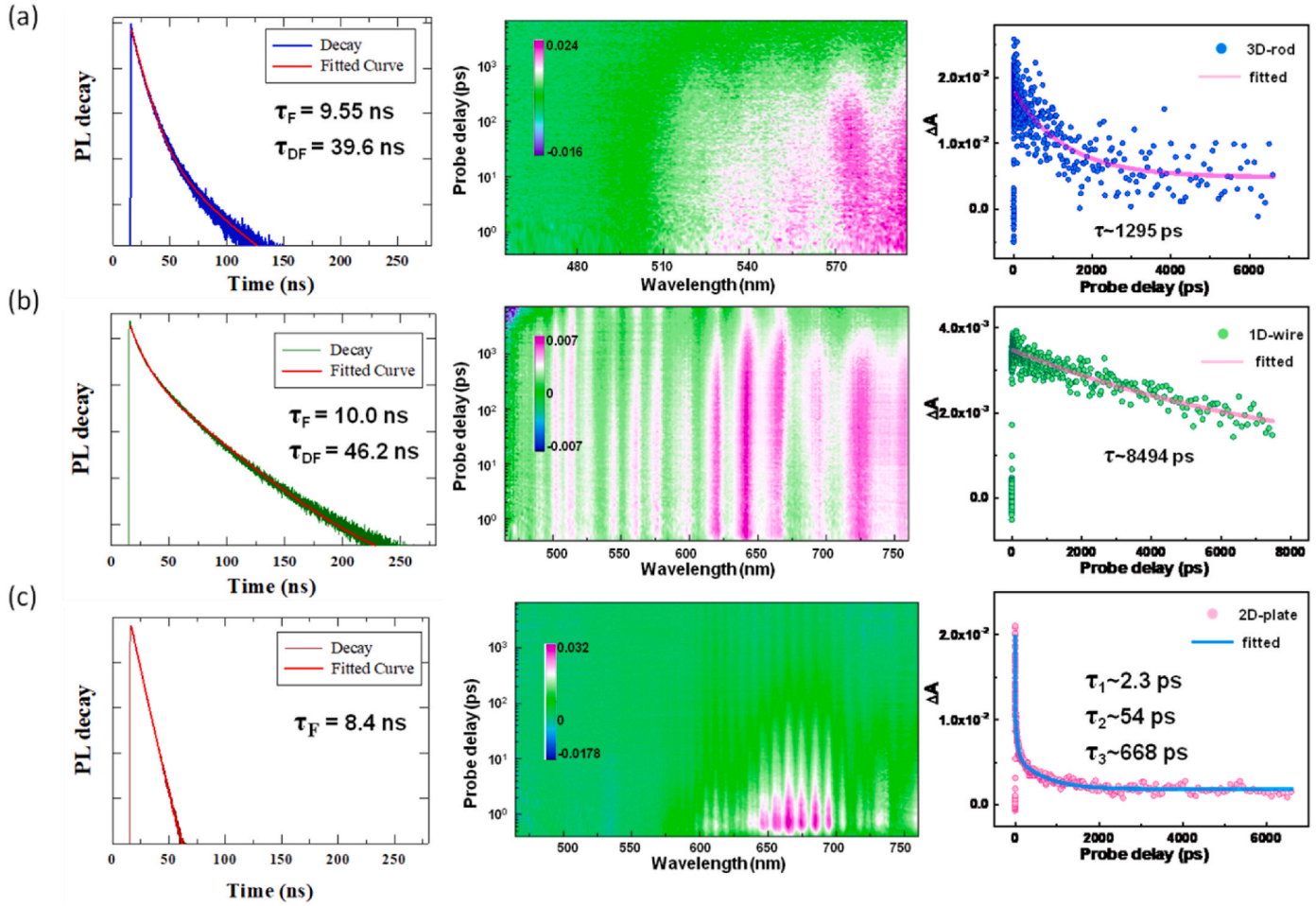

Fig. 3. Transient decay and absorption spectroscopy of (a) 3D rod (b) 1D wire and (c) 2D plate obtained under ambient conditions. (left) The red curve represents the fitted curve of the data to extract prompt and delayed emission components. (middle) Color maps of TA from three single-crystals showing the ESA feature. The vertical stripes in the ESA spectrum are caused by the interference effect of the detector due to the white light from the probe. (right) The charge carrier dynamics of the three crystals at the probe wavelength of 652 nm. (For interpretation of the references to color in this figure legend, the reader is referred to the Web version of this article.)

potential is formed from a FE and STE states [33] In the case of coronene, which adopts 3D herringbone structure, the STE state is located energetically above the lowest singlet exciton state, and the presence of the self-trapped barrier prevents the transition to the STE state [34] As the self-trapping depends strongly on the dimensionality of the materials, crystallization of coronene into thin needle leads to lowering or loss of the potential barrier, resulting in the easier formation of STE states [35]

Our results offer fresh perspectives for explaining the observed spectral features and are in partial agreement with previous research that the dimensionality of the materials and the dimensionality of structure are crucial for the formation and access of the STE state. These two types of dimensionalities can be very well understood in, for example, perovskite materials, where the materials dimensionality emphasizes the building blocks of the perovskites and the structure dimensionality emphasizes the morphologies of the materials. Namely, the perovskites can take 3D form with corner-sharing octahedra, 2D form with octahedra connected in layered sheets, 1D form with octahedra connected in chain, and 0D with isolated octahedra in their materials dimensionality. These perovskites can take 0D nanocrystal, 1D nanowires, 2D nanoplatelets, and 3D bulk form in the structure dimensionality [36] STE formation will take place in low-dimensional perovskites, in materials dimensionality, due to both long- and short-range exciton-phonon coupling enhancement [37] On the other hand, the photophysical properties remain unchanged for changing the structural dimensionality relative to the basic building blocks [38]

The three crystals discussed in this work adopts 3D herringbone structure as in materials dimensionality, which have final crystal morphologies of 3D rod, 2D plate, and 1D wire as in structure dimensionality. In the case of 3D rod and 2D plate crystals, more than 90 % of the detected emission comes from FE luminescence, attributed to singlet excitons relaxing from the lowest exciton state of the S(1) state with decay time of approximately 8–9 ns. In 1D wire crystals, 72.0 % of the observed emission comes from DF from STE below the S(1) state of coronene with a decay time of 46 ns, while only 28.0 % comes from FE luminescence from the S(1) state with a decay time of about 9.5 ns. In 1D wire, unlike the other two crystals, significant portion of excitons undergoes ESA from the S(1) state to the long-lived higher excited state, which are expected to be located energetically higher than the self-trapping barrier, resulting in the formation of STE state (Scheme 2). It should be noted here that the observed DF from 3D rod and 1D wire crystal can be also assigned to emission from excited-state dimer (excimer), which are formed when the molecule in the excited-state approaches the other molecule in ground-state, leading to the lowered potential energy curve. The emission from such excimer state often presents largely red-shifted, broad, weak and longer lifetime emission compared to the emission from monomer [39], which can be observed as a small hump at around 600 nm in their PL spectroscopy (Fig. S4). The observed spectrum is the sum of a series of many energy transitions from various vibrational levels of the ground state to various levels of the excited state. The strength of each individual transition depends on the population at the excited state. There may exist various factors, including morphology and crystal structures, that can lead to large changes in the absorption and emission properties. Further investigations are being carried out to obtain in-depth understandings of the mechanisms for the emission properties.

In organic solid, the magnitude of the exciton-phonon coupling depends on the distance between the nearest neighbor molecules [35] The fact that the intermolecular distance in 3D rod and 1D wire are the same, the formation of STE was induced independent of the magnitude of electron-phonon coupling, whereas enhancement of ESA plays key role in inducing exciton self-trapping. In general, ESA is undesired for efficient output since it does not contribute to emission intensity, where estimated PLQY is typically less than 1.0 % [10] Surprisingly, we found that the integrated intensity of PL spectroscopy for 1D wire was 27 times more than that of 3D rod. This suggests that, while most singlet excitons in 3D rod undergo ISC process to generate triplet excitons and relax non-radiatively, many singlet excitons in 1D wires undergo the ESA process before the ISC process occurs. As a result, more singlet excitons form STEs and relax back to ground state via the radiative path, resulting in significant increase in PLQY of 15.3 %. In coronene, there are possibility of enhancing further the STE formation by increasing the magnitude of exciton-phonon interaction. Organic hydrocarbon molecular crystals, unlike inorganic materials, are very flexible in their crystal packing and morphological shape, which makes them an excellent system for studying the effects of morphological alterations and crystal structure on luminescence tuning.

4. Conclusion

We synthesized coronene single-crystals: γ-polymorph 3D rod and 1D wire, and β-polymorph 2D plate coronene dimer. When exposed to

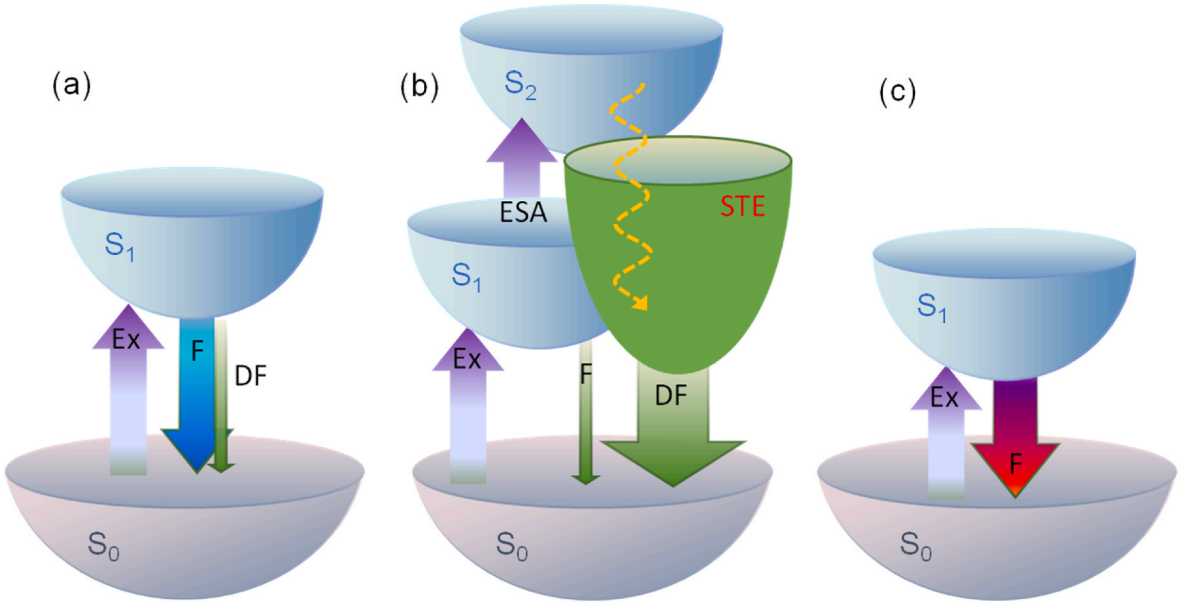

Scheme 2. Schematic representation of the excited-state dynamic process for three single-crystals.

UV light under ambient conditions, the 3D rod crystals exhibit blue emission, 1D wire exhibit green emission and 2D plate exhibit red emission, realizing RGB luminescence using single excitation wavelength. The single-crystal to single-crystal transformation from 3D rod to 1D wire, which does not involve crystal structure transition, revealed that changing crystal morphology can be key tuning parameter for inducing red-shift in emission spectroscopy. We also identified the ESA process in the 1D wire crystal as the key to accessing the STE state and enhancing luminescence. The single-crystal to single-crystal transformation from 1D wire to 2D plate, which involves coronene dimerization and crystal structure transition, resulted in significantly large red-shift to red emission due to enhancement of intermolecular interactions. The discovery of a single-component purely organic molecule that can tune the luminescence color by changing morphological dimensionality in a single step might be important for applications in variety of optoelectronic devices. Our findings obtain a new and deeper understanding of the photophysical process in organic crystals by combining static and transient spectroscopic techniques. The discovery and elucidation of crystal dimensionality-dependent luminescence tuning in organic crystals shown in this study can be extended to other systems, potentially paving the way for the development of the next generation optoelectronic materials.

[CCDC 2141267 and 2141417 contains the supplementary crystallographic data for this paper. These data can be obtained free of charge from The Cambridge Crystallographic Data Centre via www.ccdc.cam.ac.uk/data_request/cif.]

CRediT authorship contribution statement

Takeshi Nakagawa: Writing – review & editing, Writing – original draft, Methodology, Investigation, Funding acquisition, Formal analysis, Data curation, Conceptualization. **Shaohua Fu:** Writing – review & editing, Investigation, Formal analysis. **Kejun Bu:** Writing – review & editing, Investigation. **Dong Wang:** Writing – review & editing, Formal analysis. **Martina Vrankić:** Writing – review & editing, Formal analysis. **Philip Dalladay-Simpson:** Writing – review & editing, Investigation, Formal analysis, Data curation. **Xia Yin:** Writing – review & editing, Formal analysis. **Jianbo Zhang:** Writing – review & editing, Formal analysis. **Yonggang Wang:** Writing – review & editing, Formal analysis. **Xujie Lü:** Writing – review & editing, Formal analysis. **Jimin Zhao:** Writing – review & editing, Investigation, Funding acquisition. **Hokwang Mao:** Writing – review & editing, Supervision, Funding acquisition. **Yang Ding:** Writing – review & editing, Supervision, Funding acquisition.

Notes

The authors declare no competing financial interest.

Declaration of competing interest

The authors declare that they have no known competing financial interests or personal relationships that could have appeared to influence the work reported in this paper.

Acknowledgment

This work was financially supported by the Beijing Natural Science Foundation (Project No. IS24025), the National Key Research and Development Program of China (2022YFA1402301, 2021YFA1400201), the National Natural Science Foundation of China (NSFC: U2230401), CAS Project for Young Scientists in Basic Research (YSBR-059).

Appendix A. Supplementary data

Supplementary data to this article can be found online at https://doi.org/10.1016/j.carbon.2024.119873.

References

[1] W. Liu, et al., High-efficiency stretchable light-emitting polymers from thermally activated delayed fluorescence, Nat. Mater. 22 (2023) 737–745, https://doi.org/10.1038/s41563-023-01529-w.
[2] E. Kim, et al., Organic light emitting board for dynamic interactive display, Nat. Commun. 8 (2017) 14964, https://doi.org/10.1038/ncommuns14964.
[3] D.N. Congreve, et al., External quantum efficiency above 100% in a singlet-exciton-fission-based organic photovoltaic cell, Science 340 (2013) 334–337, https://doi.org/10.1126/science.1232994.
[4] J. Lee, P. Jadhav, M.A. Baldo, High efficiency organic multilayer photodetectors based on singlet exciton fission, Appl. Phys. Lett. 95 (2009) 033301, https://doi.org/10.1063/1.3182787.
[5] Y. Yang, J. Ouyang, L. Ma, J.-H. Tseng, C.-W. Chu, Electrical switching and bistability in organic/polymeric thin films and memory devices, Adv. Funct. Mater. 16 (2006) 1001–1014, https://doi.org/10.1002/adfm.200500429.
[6] O. Sachnik, et al., Elimination of charge-carrier trapping by molecular design, Nat. Mater. 22 (2023) 1114–1120, https://doi.org/10.1038/s41563-023-01592-3.
[7] R. Gómez-Bombarelli, et al., Design of efficient molecular organic light-emitting diodes by a high-throughput virtual screening and experimental approach, Nat. Mater. 15 (2016) 1120–1127, https://doi.org/10.1038/nmat4717.
[8] D.G. Bossanyi, et al., Emissive spin-0 triplet-pairs are a direct product of triplet-triplet annihilation in pentacene single crystals and anthradithiophene films, Nat. Chem. 13 (2021) 163–171, https://doi.org/10.1038/s41557-020-00593-y.
[9] O. Bolton, K. Lee, H. Kim, K.Y. Lin, J. Kim, Activating efficient phosphorescence from purely organic materials by crystal design, Nat. Chem. 3 (2011) 207–212, https://doi.org/10.1038/nchem984.
[10] X. Zhao, et al., Excited state absorption upconversion induced by structural defects for photocatalysis with a breakthrough efficiency, Angew. Chem. Int. Ed. 62 (2023) e202219214, https://doi.org/10.1002/anie.202219214.
[11] C. Yuan, et al., A π-conjugated system with flexibility and rigidity that shows environment-dependent RGB luminescence, J. Am. Chem. Soc. 135 (2013) 8842–8845, https://doi.org/10.1021/ja404198h.
[12] T. Nakagawa, et al., Full-color luminescence from single-component hydrocarbon crystal: RGB emission by altering molecular packing under pressure, Adv. Opt. Mater. 11 (2023) 2300586, https://doi.org/10.1002/adom.202300586.
[13] J.W. Chung, et al., Shear- and UV-induced fluorescence switching in stilbenic π-dimer crystals powdered by reversible [2+2] cycloaddition, J. Am. Chem. Soc. 131 (23) (2009) 8163–8172, https://doi.org/10.1021/ja900803d.
[14] A. Zavaleta, et al., Full visible spectrum and white light emission with a single, input-tunable organic fluorophore, J. Am. Chem. Soc. 142 (48) (2020) 20306–20312, https://doi.org/10.1021/jacs.0c08182.
[15] J. Ochi, K. Tanaka, Y. Chujo, Alternately π-stacked systems assisted by o-carborane: dual excimer emission and color modulation by B_{cage}-methylation, Angew. Chem. Int. Ed. 62 (2023) e202214397, https://doi.org/10.1002/anie.202214397.
[16] K. Sato, R. Katoh, Fluorescence properties of β-perylene crystals prepared by a physical vapor transport method under atmospheric pressure, Chem. Phys. Lett. 730 (2019) 312–315, https://doi.org/10.1016/j.cplett.2019.06.031.
[17] N. Fang, Y.R. Chang, D. Yamashita, et al., Resonant exciton transfer in mixed-dimensional heterostructures for overcoming dimensional restrictions in optical processes, Nat. Commun. 14 (2023) 8152, https://doi.org/10.1038/s41467-023-43928-2.
[18] J. Potticary, et al., An unforeseen polymorph of coronene by application of magnetic fields during crystal growth, Nat. Commun. 7 (2016) 11555, https://doi.org/10.1038/ncommuns11555.
[19] A. Neef, et al., Orbital-resolved observation of singlet fission, Nature 616 (2023) 275–279, https://doi.org/10.1038/s41586-023-05814-1.
[20] A.J. Gillett, et al., The role of charge recombination to triplet excitons in organic solar cells, Nature 597 (2021) 666–671, https://doi.org/10.1038/s41586-021-03840-5.
[21] H. Uoyama, et al., Highly efficient organic light-emitting diodes from delayed fluorescence, Nature 492 (2012) 234–238, https://doi.org/10.1038/nature11687.
[22] J. Robertson, J. White, Crystal structure of coronene, Nature 154 (1944) 605, https://doi.org/10.1038/154605a0.
[23] R. Goddard, et al., Crystallization of large planar polycyclic aromatic hydrocarbons: the molecular and crystal structures of hexabenzo[bc,ef,hi,kl,no,qr] coronene and Benzo[1,2,3-bc:4,5,6-b'c']dicoronene, J. Am. Chem. Soc. 117 (1995) 30–41, https://doi.org/10.1021/ja00106a004.
[24] X. Zhao, et al., Phase transformations and vibrational properties of coronene under pressure, J. Chem. Phys. 139 (2013) 144308, https://doi.org/10.1063/1.4824384.
[25] B. Botka, et al., Interactions and chemical transformations of corornene inside and outside carbon nanotubes, Small 10 (2014) 1369–1378, https://doi.org/10.1002/small.201302613.
[26] P. Kubelka, F.A. Munk, Ein Beitrag zur Optik der Farbanstriche. Z. Techn, Phys. 12 (1931) 593–601.
[27] S. Hirata, Recent advances in materials with room temperature phosphorescence: photophysics for triplet exciton stabilization, Adv. Opt. Mater. (2017) 1700116, https://doi.org/10.1002/adom.201700116.
[28] T. Nakagawa, et al., Piezochromic luminescence of dicoronylene: key for revealing hidden Raman modes at high pressure, Carbon 197 (2022) 563–569, https://doi.org/10.1016/j.carbon.2022.06.009.

[29] M. Sun, O. Anhalt, M.B. Sárosi, M. Stolte, F. Würthner, Activating Organic Phosphorescence via Heavy Metal–π Interaction Induced Intersystem Crossing, Adv. Mater. 34 (2022) 202207331. https://doi.org/10.1002/adma.202207331.
[30] J.L. Kropp, W.R. Dawson, Radiationless deactivation of triplet coronene in plastics, J. Phys. Chem. 71 (13) (1967) 4499–4506, https://doi.org/10.1021/j100872a054.
[31] J. Potticary, T.T. Jensen, S.R. Hall, Nanostructural origin of blue fluorescence in the mineral karpatite, Sci. Rep. 7 (2017) 9867, https://doi.org/10.1038/s41598-017-10261-w.
[32] A.H. Matsui, K. Mizuno, Crystallization and excitonic luminescence of coronene crystals, J. Phys. D Appl. Phys. 26 (1993) B242–B244, https://doi.org/10.1088/0022-3727/26/8B/042.
[33] A.H. Matsui, Excitonic processes in aromatic molecular crystals of strong exciton-phonon coupling, Pure Appl. Chem. 67 (1995) 429–436, https://doi.org/10.1351/pac199567030429.
[34] S. Nakatani, T. Nakamura, K. Mizuno, A.H. Matsui, Interband and intraband exciton scattering in coronene crystal, J. Lumin. 58 (1994) 343–346, https://doi.org/10.1016/0022-2313(94)90432-4.
[35] M. Sakurai, M. Furukawa, K. Mizuno, A. Matsui, Free-exciton luminescence and weak-exciton scattering in coronene crystals, J. Phys. Soc. Jap. 61 (1992) 445–448, https://doi.org/10.1143/JPSJ.61.445.
[36] S. Gonzalez-Carrero, R.E. Galian, J. Perez-Prieto, Maximizing the emissive properties of $CH_3NH_3PbBr_3$ perovskite nanoparticles. Part, Part. Syst. Char. 32 (2015) 709–720. https://doi.org/10.1039/C4TA05878J.
[37] Y. Zhang, L. Zhu, Z. Yang, W. Tao, Z. Chen, T. Li, H. Lei, C. Li, L. Wang, W. Tian, Z. Li, H. Shang, H. Zhu, Transient photoinduced Pb^{2+} disproportionation for exciton self-trapping and broadband emission in low-dimensional lead halide perovskites, J. Am. Chem. Soc. 146 (11) (2024) 7831–7838. https://doi.org/10.1021/jacs.4c01115.
[38] Z. Yuan, C. Zhou, Y. Tian, J. Messier, J.C. Wang, L.J. van de Burgt, K. Kountouriotis, Y. Xin, E. Holt, K. Schanze, R. Clark, T. Siegrist, B. Ma, One-dimensional organic lead halide perovskites with efficient bluish white-light emission, Nat. Commun. 8 (2017) 14051. https://doi.org/10.1038/ncomms14051.
[39] O.P. Dimitriev, Y.P. Piryatinski, Y.L. Slominski, J. Phys. Chem. Lett. 9 (9) (2018) 2138–2143. https://doi.org/10.1021/acs.jpclett.8b00481.